Generation and characterization of adjustable pure third-order spatial phase by tuning optical aberrations

Daryoush Abdollahpour,[1,2,*] Morteza Lotfollahi,[1] Mohammad Yeganeh,[1] and Saifollah Rasouli[1,2]

[1] *Department of Physics, Institute for Advanced Studies in Basic Sciences (IASBS), Zanjan 45137-66731, Iran*
[2] *Optics Research Center, Institute for Advanced Studies in Basic Sciences (IASBS), Zanjan 45137-66731, Iran*

(Dated: March 21, 2019)

Generation of pure third-order spatial phase is the top requirement for the generation of Airy beams through Fourier-space beam shaping method. Utilizing coma aberration for inducing such a phase profile is shown to be one of the most appropriate approaches because of providing continuous phase, capability of working at high laser powers, and low costs. Here, we demonstrate pure tunable third-order spatial generation through aberration control in a positive one-dimensional tilted cylindrical telescopic system, and experimentally verify its quality and tunability by two independent wavefront sensing methods namely moiré deflectometry and four-step phase-shifting interferometry. The deflectometry method is used for a real-time visual assessment of the quality of the imprinted wavefront, and also for a quantitive analysis of the wavefront and its dependency on the parameters of the system, while, the interferometric method is used for a more rigorous measurement of the generated wavefront. It is shown that by changing the tilt angle of the system, modulation depth of the cubic phase can be tuned. It is also shown that nearly-complete third-order form of the imprinted phase over a large aperture results in high-quality Airy beam generation.

I. INTRODUCTION

Airy beams are a new class of non-diffracting beams with peculiar and interesting properties such as curved trajectory and self-healing. Since their realization in optics by Siviloglou et al [1, 2], optical Airy beams and pulses have been the subject of tremendous investigations for various applications such as in curved plasma channel guidance [3, 4], generation of tunable intense light filaments [5], generation of light bullets [6–9], optical micro-manipulation [10–12], and recently in light-sheet microscopy [13, 14], to name a few. The electric field envelope of a one-dimensional finite energy Airy beam at an initial propagation distance ($\zeta = 0$) can be described as [1, 2]

$$u(s, \zeta = 0) = \mathrm{Ai}(s)\exp(as), \tag{1}$$

where $s = x/x_0$ is a normalized transverse dimension, x_0 is an arbitrary scale factor, a is an exponential truncation factor, and $\mathrm{Ai}(\cdot)$ represents the Airy function. The angular Fourier spectrum of this field envelope in the normalized $k-$space is a Gaussian distribution with a third-order phase modulation [1, 2]. This simply suggests that an Airy beam can be generated by imprinting a third-order spatial phase on a Gaussian beam and performing a Fourier transformation by a converging lens or free-space propagation over a long distance. Several methods have been used for generating spatial third-order phase such as utilizing liquid crystal spatial light modulators (SLMs) (for instance in [1, 2]), permanent optical phase masks [3, 15], three-wave mixing in asymmetric nonlinear photonic crystals [16], optical aberrations [5, 14, 17] and specially designed optical elements with cubic surface profiles [9, 18]. In addition, it has been shown that laterally non-spreading ultrabroadband Airy wavepackets can be achieved by continuous cubic phase profiles [9] while discontinuities in the phase profile created by spatial light modulators lead to lateral spreading of the wavepacket [19]. Moreover, permanent phase masks are not tunable and are usually very expensive. Similarly, surfaces with cubic profiles are difficult to fabricate and often also very expensive. On the other hand, Papazoglou, et al. [5], have proposed and demonstrated that by tuning optical aberrations in a tilted cylindrical telescopic system, composed of a negative and a positive cylindrical lens, the coma aberration, which results in third-order phase profile can be isolated and maintained in the system while other aberrations nearly cancel out each other. This relatively simple and low-cost method is indeed capable of providing adjustable continuous phase profile at high input laser powers. Moreover, using a cubic phase distribution in a wavefront-coding imaging scheme is shown to provide a fast volumetric imaging capability, by extending depth-of-field of the imaging system, for monitoring dynamical processes [20, 21].

Nevertheless, obtaining a pure third-order spatial phase in the Fourier-space for generating exponentially truncated Airy beams through tuning aberrations in a tilted telescopic system is a very delicate task since unbalanced second- or forth-order (and even higher order) phase terms, lead to beam degradation and significantly alter its propagation. To ensure that the desired phase profile is achieved for a given set of alignment parameters of the system, the generated Fourier-space wavefront has to be inspected by a wavefront sensing method.

Here, we introduce a positive tilted cylindrical telescopic system composed of two identical positive cylindri-

* Corresponding author: dabdollahpour@iasbs.ac.ir

cal lenses for imprinting pure cubic phase (i.e. in a complete cubic polynomial form) in one- and two-dimensions. Our proposed system can be utilized in various experimental situations for different applications, since the system proposed in [5] is relatively tightly spaced. Moreover, not content with simulations of the obtained wavefronts, as it may differ from the practically generated ones, in order to inspect the generated wavefront and its dependencies on different parameters of the system, a wavefront sensor based on two-channel moiré deflectometry, for quick monitoring of the wavefront, and a four-step phase-shifting interferometry scheme, for verification of the results obtained by the quick measurement, were developed and used.

II. DESIGN AND EXPERIMENT

As depicted in Fig. 1(a), the tilted telescopic system is composed of two identical positive plano-convex cylindrical lenses of a width of 4.2 cm, and a focal distance of $f = 15$ cm. The first lens is mounted in a way that its tilt angle, θ, and transverse offset, t_1, with respect to the incident beam axis could be tuned. The longitudinal position of the second lens with respect to the first lens, d, and its transverse offset with respect to the initially collimated beam, t_2, were adjusted by a two-dimensional translation stage. Simple ray-tracing analysis show that for specific alignment parameters (i.e. θ, d, t_1 and t_2), a pure cubic phase profile can be imprinted on a Gaussian beam incident on the lower half of the first lens (see Fig. 1), since an efficient canceling of the second and fourth order spatial phases is achieved only when the beam is incident on the lower half of the first lens. Moreover, a two-dimensional third-order phase can be obtained by placing an orthogonally oriented second tilted cylindrical telescopic system after the first one, as shown in Fig. 1(b).

The experimental setup for generation and characterization of the desired phase profile is depicted in Fig. 2. The output of a He-Ne laser ($\lambda = 632.8$ nm) was spatially filtered and collimated to a FWHM of 12 mm

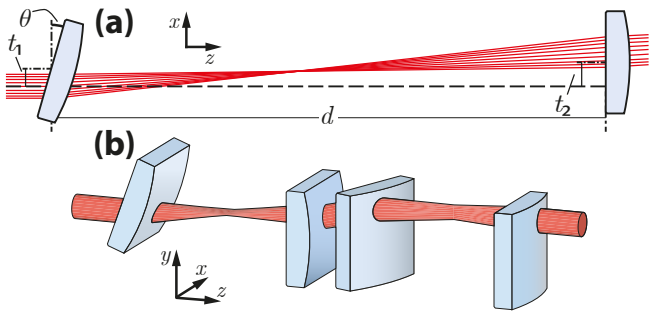

FIG. 1. Schematics of the tilted cylindrical telescopic system(s) for generating third-order spatial phase in one- and two-dimensions ((a) and (b), respectively).

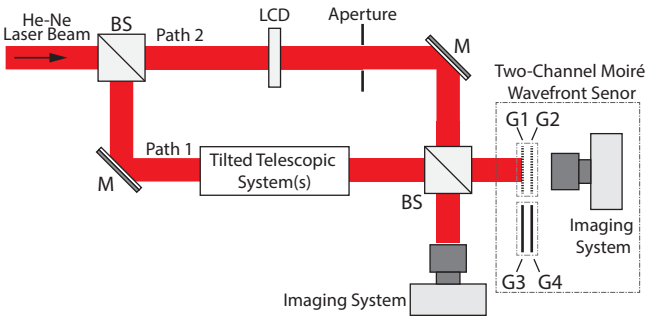

FIG. 2. Schematic of the experimental setup. The tilted telescopic system is placed in *path 1* and it is followed by a two-channel moiré wavefront sensor composed of four gratings and an imaging system. *Path 2* is mainly designed for phase-shifting interferometric wavefront sensing where an LCD is used to provide required phase shifts. BS: beam splitter; M: mirror; LCD: liquid crystal display; G1, G2, G3 and G4: gratings.

and then split in two paths. *Path 1* includes the tilted telescopic system followed by a two-channel moiré wavefront sensor, while *path 2* is mainly used for interferometric wavefront sensing based on phase-shifting interferometry where a computer-controlled liquid-crystal display (LCD) was utilized to provide required phase shifts.

Each channel of the moiré wavefront sensor is composed of a sequence of two identical Ronchi amplitude gratings slightly rotated with respect to each other, in their respective transverse planes, and longitudinally separated by a positive integer multiple of the Talbot distance. In this setup, gratings G1 and G2 form the $x-$channel, while G3 and G4 (both orthogonally oriented with respect to G1 and G2) form the $y-$channel. For an incident plane-wave, moiré pattern in each channel is consisted of parallel fringes of period d_m orthogonally oriented with respect to the fringes of the other channel. Upon a change in the wavefront of the incident wave, fringes are locally displaced by $\Delta x_m(x,y)$ and $\Delta y_m(x,y)$ along x and y directions, respectively; through which wavefront gradients can be obtained as [22]

$$\left[\frac{\partial\phi(x,y)}{\partial x}, \frac{\partial\phi(x,y)}{\partial y}\right] = \frac{d_g}{d_m z_N}\left[\Delta y_m, \Delta x_m\right], \qquad (2)$$

where d_g is the period of the gratings and $z_N = N(2d_g^2/\lambda)$ is the N^{th} integer multiple of the Talbot distance for a collimated beam of a wavelength λ. Thus, wavefront reconstruction can be performed by measuring the local displacement of the moiré fringes and integration over x and y dimensions. As shown in Fig. 3(e-f), for a nearly cubic phase profile in one-dimension (e.g. along x-axis), moiré fringe pattern in x-channel transforms to a set of nearly parabolic fringes, while they remain unaltered in y-channel, in the form of straight vertical parallel lines (not shown). Therefore, for examination of the cubic phase generation only in one-dimension a single channel wavefront sensor would suffice. Additionally, investi-

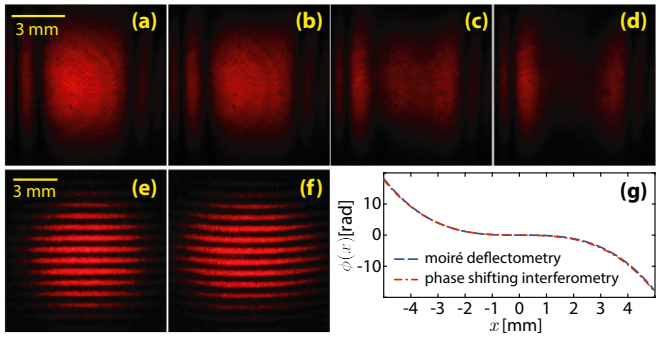

FIG. 3. Four-step phase-shifting interference patterns corresponding to phase shifts of 0, -0.25π, -0.46π, and -0.70π (a-d, respectively); $x-$channel moiré fringes of a collimated beam, (e), and a beam with a cubic phase profile along $x-$axis, (f). (g) Retrieved phase profiles along $x-$axis by the two methods. All figures present experimental data corresponding to a tilt angle of $\theta = 16°$.

gation of a time-independent two-dimensional wavefront can be performed sequentially and separately by each channel (as in our case). For two-dimensional nearly cubic phase profile, fringes in both channels have parabolic paths along their respective axes. It is important to note that a qualitative assessment of the purity of the imprinted cubic phase, can simply be performed by visual monitoring of the goodness of a parabolic fit on the moiré fringe paths, without the need for further quantitative analysis. Nevertheless, for such a simple fringe system, extraction of fringe paths followed by a numerical integration for wavefront reconstruction could be performed within a very short time. Therefore, the role of the alignment parameters of the positive tilted telescopic system on the output phase profile could be monitored almost in real-time. For the experiments, we used identical gratings of period $d_g \approx 66.7\mu$m longitudinally separated by twice the Talbot distance (i. e. $z_2 = 2.8$ cm). In addition, since an interferometric approach would, in principle, reveal the wavefront more precisely, we also measured the wavefront by four-step phase-shifting interferometry. As shown in Fig. 2, the telescopic system was placed in *path 1* of a Mach-Zehnder interferometer, while an LCD (1024×768 pixels, and pixel size of 13 μm), capable of providing a desired uniform phase shift of up to $\sim\pi$ on the whole beam, was placed in the other arm (*path 2*). The zeroth-order diffraction from the LCD was allowed to interfere with the beam from *path 1*. Interference patterns associated to four phase steps of 0, -0.25π, -0.46π and -0.70π (Fig. 3(a-d)), (I_1, I_2, I_3 and I_4, respectively), were captured separately and the phase profile was calculated as

$$\phi(x,y) = \arctan\left[\frac{1}{c_3}\left(\frac{1}{\eta - c_1} + c_2\right)\right], \qquad (3)$$

where $\eta = (I_1 - I_3)/(I_2 - I_4)$, $c_1 = 11.9504$, $c_2 = 0.0887$, and $c_3 = 0.0056$. It should be noted that in contrary to the moiré wavefront sensing, the interferometric measurement can not be performed at once since multiple interference patterns, associated to the four phase steps, are to be acquired separately. As monitored by the moiré wavefront sensor, for a range of tilt angles of the first lens pure cubic phase profiles could be achieved when transverse offsets of the first and the second lenses where fixed at $t_1 = 7.5$ mm, and $t_2 = 14$ mm, respectively, and their longitudinal separation distance, d, was tuned. In such a situation, generated phase profile was measured by the methods for several tilt angles. Retrieved phase profiles, for a tilt angle of $\theta = 16°$ and longitudinal separation distance of $d = 271.3$ mm, are shown in Fig. 3(g). A good agreement between the results of the two methods can be easily seen.

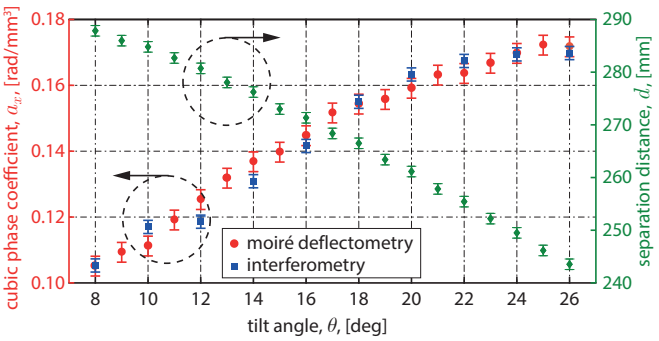

FIG. 4. Experimentally retrieved cubic phase coefficients, and optimum separation distances between the lenses in a 1D system for several tilt angles of the first lens.

III. RESULTS AND DISCUSSION

For several tilt angles of the first lens, and the same transverse positions of the lenses, separation distance was adjusted to achieve a pure cubic phase. A one-dimensional cubic function in the form of $\phi(x) = a_x(x - x_0)^3 + \phi_0$, was then fitted on independently retrieved phase profiles, where ϕ_0 is a constant phase, a_x is a cubic phase coefficient and x_0 is the center coordinate of the wavefront. Cubic phase coefficient of the pure cubic phase distributions along with optimum separation distance between the lenses as a function of the tilt angle are depicted in Fig. 4. It is evidently seen that for the fixed transverse positions of the lenses, a tunable pure cubic phase can be achieved by adjusting the tilt angle of the first lens and separation distance of the lenses. It should be added that, as another mean of tuning the wavefront, using identical cylindrical lenses with shorter focal lengths would result in more steep wavefront gradients and thus greater cubic coefficients. On the other hand, useful aperture size of the system for generating cubic phase profile is limited to half width of the lenses.

Moreover, for cubic phase generation in two-dimensions, two tilted telescopic systems were built separately with tilt angles of $\theta_y = 16°$ and $\theta_x = 14°$. Trans-

verse offsets of the lenses with respect to incident beam in each system were adjusted in a way that each one could imprint a cubic phase in its respective direction. The systems were then oriented orthogonally (as depicted in Fig. 1(b)) and placed in tandem with a separation distance of 4.5 cm. Contours of the retrieved wavefront (in waves) by using the interferometric method are shown in Fig. 5 along with the contours of a cubic polynomial fit in the form of $\phi(x,y) = \phi_0 + a_x(x-x_0)^3 + a_y(y-y_0)^3$, where ϕ_0 is a constant phase, a_x, a_y are cubic phase coefficients for x and y directions, and (x_0, y_0) are the coordinates of the center of the wavefront. The best fit to the retrieved wavefront is achieved with $a_x = -0.144$ rad/mm^3 and $a_y = -0.132$ rad/mm^3. It is evidently seen that the maximum deviation from a perfect cubic polynomial is less than $\lambda/4$. It should be noted that the constant phase and the central coordinates of the wavefront are of no importance for practical use.

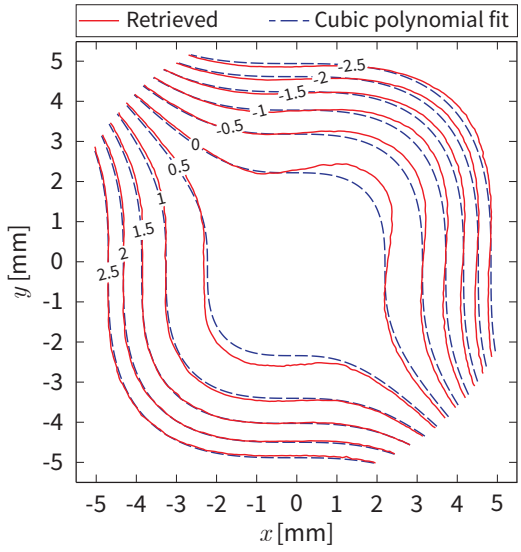

FIG. 5. Contour plot of the experimentally imprinted two-dimensional phase profile (in waves), by a cascade of two tilted telescopic systems with $\theta_x = 14^\circ$ and $\theta_y = 16^\circ$; solid curves: retrieved phase profile by using the interferometric technique and dashed curves: cubic polynomial fit.

Furthermore, generated one- and two-dimensional Airy beam profiles and their propagation were inspected as well. Generated beam profiles along with a measurement of the propagation trajectory of the 1D Airy beam are depicted in Fig. 6. For generation of the 1D Airy beam (Fig. 6(a)), the tilt angle was set to 16° and an additional cylindrical lens with the focal length of $f = 15$ cm was placed 15 cm after the second lens of the telescopic system for one-dimensional spatial Fourier transformation. A 1D Airy beam was formed near the focal plane of the Fourier lens and its propagation was inspected by imaging the transverse beam profile along the propagation direction by using a CCD mounted on a translation stage. Transverse displacement of the main lobe of the Airy beam around the focal plane of the Fourier lens (i.e. $z = 0$) is shown in Fig. 6(c). In comparison to the parabolic fit, it is clearly seen that the propagation trajectory is a parabolic path. Moreover, the transverse profile of a 2D Airy beam generated by a cascade of two tilted telescopic systems with tilt angles of $\theta_x = 14^\circ$ and $\theta_y = 17^\circ$ and by using a spherical Fourier lens with a focal length of 1 m is shown in Fig. 6(b). Clearly, the generated beam is of a very high quality with a very small exponential truncation factor of $a = 0.025$. Moreover, both of the generated beams exhibit self-healing as expected (data not shown).

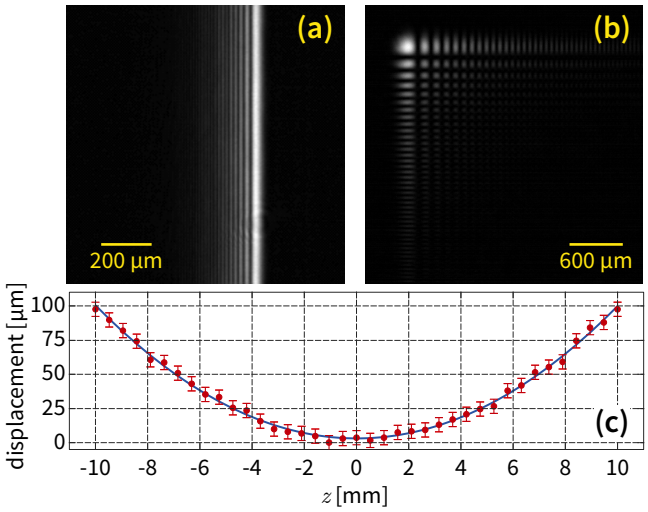

FIG. 6. Experimentally generated beam profiles and their propagation. Generated 1D (a) and 2D (b) Airy beam profiles, and parabolic propagation path of the 1D Airy beam around the focal plane of the Fourier lens (c); solid curve represents a parabolic fit.

IV. CONCLUSION

In conclusion, we have presented a positive tilted telescopic system for generating tunable continuous spatial cubic phase in one- and two-dimensions through isolation of coma aberration in the system. Quality and adjustability of the generated phase profiles are assessed by two independent wavefront sensing methods, moiré deflectometry and four-step phase-shifting interferometry. Moiré deflectometry is firstly used as a real-time visual monitoring tool of the imprinted phase and its dependency on various parameters of the system. Moreover, a quantitive measurement of the wavefronts were performed by both methods for various tilt angle of the first lens and optimum separation distance between the two lenses in the 1D system, and a good agreement between the results is observed. Our wavefront sensing results indicate that by adjusting the tilt angle of the first lens in the telescopic system, generated cubic phase can be tuned. Furthermore, we have shown that as a result of effective isolation of third-order phase term over a wider aperture in

the proposed system, resultant Airy beams are of a very high quality both in one- and two-dimensions. The system can be used in various applications including generation of high-power high-quality Airy beams and extended depth-of-field imaging in several microscopy techniques.

[1] G. A. Siviloglou, J. Broky, A. Dogariu, and D. N. Christodoulides, Phys. Rev. Lett. **99**, 213901 (2007).
[2] G. A. Siviloglou and D. N. Christodoulides, Opt. Lett. **32**, 979 (2007).
[3] P. Polynkin, M. Kolesik, J. V. Moloney, G. A. Siviloglou, and D. N. Christodoulides, Science **324**, 229 (2009).
[4] M. Clerici, Y. Hu, P. Lassonde, C. Milián, A. Couairon, D. N. Christodoulides, Z. Chen, L. Razzari, F. Vidal, F. Légaré, D. Faccio, and R. Morandotti, Science Advances **1** (2015), 10.1126/sciadv.1400111.
[5] D. G. Papazoglou, S. Suntsov, D. Abdollahpour, and S. Tzortzakis, Physical Review A **81**, 061807 (2010).
[6] A. Chong, W. H. Renninger, D. N. Christodoulides, and F. W. Wise, Nat Photon **4**, 103 (2010).
[7] D. Abdollahpour, S. Suntsov, D. G. Papazoglou, and S. Tzortzakis, Physical Review Letters **105**, 253901 (2010).
[8] T. J. Eichelkraut, G. A. Siviloglou, I. M. Besieris, and D. N. Christodoulides, Optics Letters **35**, 3655 (2010).
[9] A. Valdmann, P. Piksarv, H. Valtna-Lukner, and P. Saari, Optics Letters **39**, 1877 (2014).
[10] J. Baumgartl, M. Mazilu, and K. Dholakia, Nat Photon **2**, 675 (2008).
[11] P. Zhang, J. Prakash, Z. Zhang, M. S. Mills, N. K. Efremidis, D. N. Christodoulides, and Z. Chen, Optics Letters **36**, 2883 (2011).
[12] Z. Zheng, B.-F. Zhang, H. Chen, J. Ding, and H.-T. Wang, Applied Optics **50**, 43 (2011).
[13] T. Vettenburg, H. I. C. Dalgarno, J. Nylk, C. Coll-Llado, D. E. K. Ferrier, T. Cizmar, F. J. Gunn-Moore, and K. Dholakia, Nat Meth **11**, 541 (2014).
[14] Z. Yang, M. Prokopas, J. Nylk, C. Coll-Lladó, F. J. Gunn-Moore, D. E. K. Ferrier, T. Vettenburg, and K. Dholakia, Biomed. Opt. Express **5**, 3434 (2014).
[15] P. Polynkin, M. Kolesik, and J. Moloney, Physical Review Letters **103**, 123902 (2009).
[16] T. Ellenbogen, N. Voloch-Bloch, A. Ganany-Padowicz, and A. Arie, Nat Photon **3**, 395 (2009).
[17] Z. Cao, C. Zhai, J. Li, F. Xian, and S. Pei, Optics Communications **393**, 11 (2017).
[18] B. Yalizay, B. Soylu, and S. Akturk, J. Opt. Soc. Am. A **27**, 2344 (2010).
[19] P. Piksarv, A. Valdmann, H. Valtna-Lukner, R. Matt, and P. Saari, Opt. Lett. **38**, 1143 (2013).
[20] O. E. Olarte, J. Andilla, D. Artigas, and P. Loza-Alvarez, Optica **2**, 702 (2015).
[21] S. Quirin, N. Vladimirov, C.-T. Yang, D. S. Peterka, R. Yuste, and M. B. Ahrens, Opt. Lett. **41**, 855 (2016).
[22] M. Yeganeh, S. Rasouli, M. Dashti, S. Slussarenko, E. Santamato, and E. Karimi, Opt. Lett. **38**, 887 (2013).